

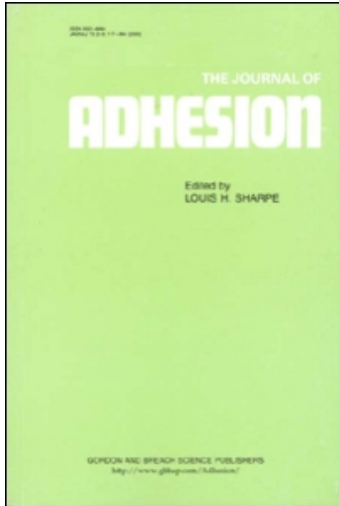
This article was downloaded by:

On: 22 January 2011

Access details: *Access Details: Free Access*

Publisher *Taylor & Francis*

Informa Ltd Registered in England and Wales Registered Number: 1072954 Registered office: Mortimer House, 37-41 Mortimer Street, London W1T 3JH, UK



The Journal of Adhesion

Publication details, including instructions for authors and subscription information:

<http://www.informaworld.com/smpp/title~content=t713453635>

Three-dimensional finite element analysis of stress response in adhesive butt joints subjected to impact bending moments

Izumi Higuchi^a; Toshiyuki Sawa^b; Hirohisa Okuno^b; Shinya Kato^b

^a Josai High School, Kofu, Yamanashi, Japan ^b Yamanashi University, Takeda, Kofu, Yamanashi, Japan

Online publication date: 08 September 2010

To cite this Article Higuchi, Izumi , Sawa, Toshiyuki , Okuno, Hirohisa and Kato, Shinya(2010) 'Three-dimensional finite element analysis of stress response in adhesive butt joints subjected to impact bending moments', *The Journal of Adhesion*, 79: 11, 1017 – 1039

To link to this Article: DOI: 10.1080/714906154

URL: <http://dx.doi.org/10.1080/714906154>

PLEASE SCROLL DOWN FOR ARTICLE

Full terms and conditions of use: <http://www.informaworld.com/terms-and-conditions-of-access.pdf>

This article may be used for research, teaching and private study purposes. Any substantial or systematic reproduction, re-distribution, re-selling, loan or sub-licensing, systematic supply or distribution in any form to anyone is expressly forbidden.

The publisher does not give any warranty express or implied or make any representation that the contents will be complete or accurate or up to date. The accuracy of any instructions, formulae and drug doses should be independently verified with primary sources. The publisher shall not be liable for any loss, actions, claims, proceedings, demand or costs or damages whatsoever or howsoever caused arising directly or indirectly in connection with or arising out of the use of this material.

THREE-DIMENSIONAL FINITE ELEMENT ANALYSIS OF STRESS RESPONSE IN ADHESIVE BUTT JOINTS SUBJECTED TO IMPACT BENDING MOMENTS

Izumi Higuchi

Josai High School, Kofu, Yamanashi, Japan

Toshiyuki Sawa

Hirohisa Okuno

Shinya Kato

Yamanashi University, Takeda, Kofu, Yamanashi, Japan

The stress wave propagation and the stress distribution in adhesive butt joints of T-shaped similar adherends subjected to impact bending moments are calculated using a three-dimensional finite-element method (FEM). An impact bending moment is applied to a joint by dropping a weight. The FEM code employed is DYNA3D. The effects of the Young's modulus of adherends, the adhesive thickness, and the web length of T-shaped adherends on the stress wave propagation at the interfaces are examined. It is found that the highest stress occurs at the interfaces. In the case of T-shaped adherends, it is seen that the maximum principal stress at the interfaces increases as Young's modulus of the adherends increases. In the special case where the web length of T-shaped adherends equals the flange length, the maximum principal stress at the interfaces increases as Young's modulus of the adherends decreases. The maximum principal stress at the interfaces increases as the adherend thickness decreases. The characteristics of the T-shaped adhesive joints subjected to static bending moments are also examined by FEM and compared with those under impact bending moments. Furthermore, strain response of adhesive butt joints was measured using strain gauges. A fairly good agreement is observed between the numerical and the experimental results.

Keywords: FEM; Stress response; Impact bending moments; T-shaped adhesive joints; Interface; Three-dimensional; Strain measurement; Maximum principal stress; Stress singularity

Received 5 September 2001; in final form 15 August 2003.

Hirohisa Okuno is presently at NKK Co. Ltd, Japan.

Shinya Kato is presently at Nippon Denso Co. Ltd, Japan.

Address correspondence to Toshiyuki Sawa, Yamanashi University, 4-3-11, Takeda, Kofu, Yamanashi, 400-0016, Japan. E-mail: sawa@ccn.yamanashi.ac.jp

INTRODUCTION

Adhesive joints have been used in mechanical structures, the automobile and aerospace industries, electric devices, and so on. Some studies [1–10] have been carried out on the stress distribution of adhesive joints under static loadings such as tensile loads, bending moments, and cleavage loads. Recently, adhesive joints in automobile structures have been used under impact loadings as well as static loadings. However, little research [11–16] has been done on mechanical behavior of adhesive joints under impact loadings. Higuchi et al. have reported on the stress propagation of adhesive butt joints of T-shaped adherends subjected to impact tensile loads [14]. In addition, it has been found that the characteristics of adhesive butt joints under impact loadings are different from those under static loadings. In practice, it is necessary to know the stress propagation and the stress distribution of adhesive joints subjected to impact bending moments from a reliable design standpoint, and to know the difference in the characteristics of adhesive butt joints under impact and static loadings.

In this article, the stress wave propagation and the stress distribution in adhesive butt joints of T-shaped similar adherends subjected to impact bending moments were analyzed using a three-dimensional finite-element method. The code employed was DYN3D [17–19]. An impact four-point bending moment was applied to a joint by dropping a weight. The finite-elements method (FEM) calculations were performed in elastic deformation, and it was assumed that the strain rate of the adhesive was small. The effects of the Young's modulus of adherends, the adhesive thickness, and the geometry of T-shaped adherends on the stress wave propagation at the interfaces were examined. Furthermore, the characteristics of adhesive butt joints of T-shaped joints subjected to static bending moments were examined by FEM(MARC). The characteristics of the joints under the impact bending moments were compared with those under the static bending moments. For verification of the FEM calculations, strain response of joints subjected to impact bending loads was measured. The numerical results are compared with the measured results.

FINITE ELEMENT CALCULATIONS

Figure 1 shows a model for FEM calculations of a T-shaped adhesive butt joint. The Cartesian coordinate system (x, y, z) is used as shown in Figure 1. Pins are inserted into the inner holes of the adherends (Solid 1 & 3) shown in Figure 1 to attach a U-shaped object to the specimen. Taking the symmetry of the joint about the axis $z = 0$ into

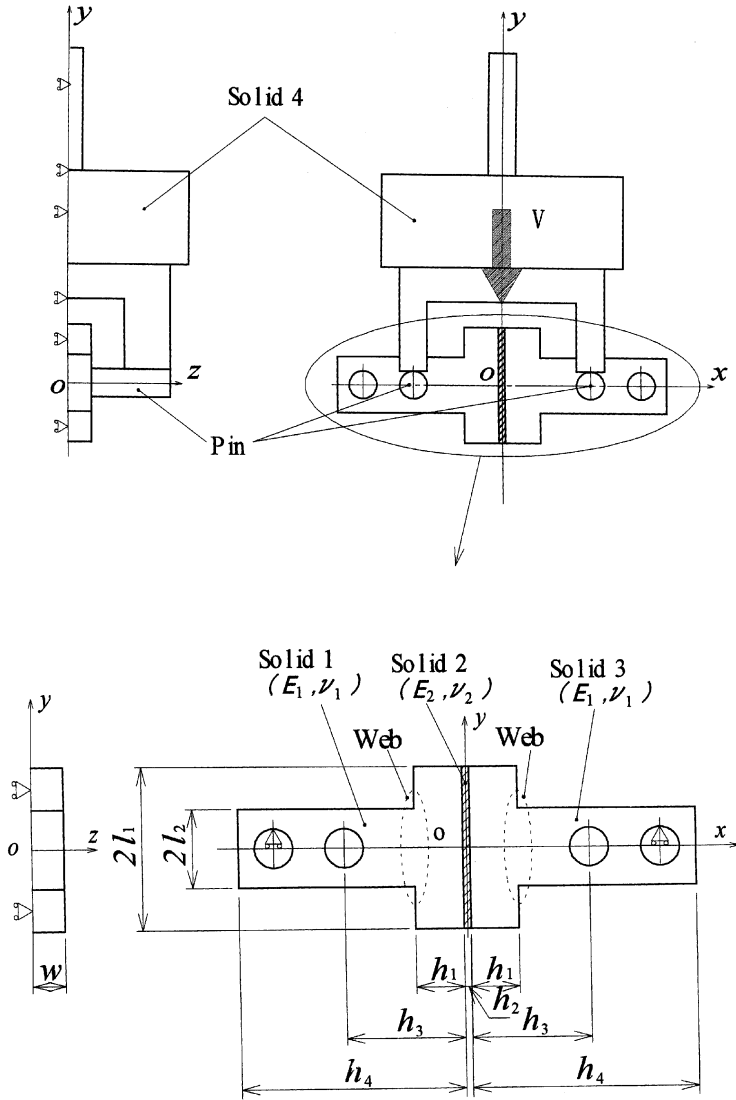


FIGURE 1 A model for analysis of T-shaped adhesive butt joints subjected to impact four-point bending moments.

consideration, one-half of the joint is analyzed. The boundary conditions are as follows: (1) the nodal points in the symmetric face are fixed in the z direction, (2) the nodal points of the upper edge in the outer hole of the adherends (Solid 1 & 3) are fixed in the y direction

TABLE 1 The Material Properties for the Adherends and the Adhesive Used in this Study

	Adherend Al6063	Adhesive Scotch-Weld1838 [®]
Young's modulus E (GPa)	69.6	3.63
Poisson's ratio ν	0.31	0.38
Density ρ (kg/mm ³)	2.66×10^{-6}	1.12×10^{-6}

shown in Figure 1b and (3) an impact load [14] is applied to the joint providing an initial velocity, v , at the weight (Solid 4) as shown in Figure 1. The flange height of the T-shaped adherends, the adhesive thickness, the height of adherends, the distance of the inner holes from the interfaces, the length of the flange, the web length, and the thickness in the x direction are denoted by h_1 , h_2 , h_3 , h_4 , $2l_1$, $2l_2$ (web length), and $2w$, respectively. Young's modulus and Poisson's ratio of adherends are denoted by E_1 and ν_1 and those of adhesive by E_2 and ν_2 , respectively. Table 1 lists the material properties of the adherends and the adhesive.

Figure 2 shows an example of mesh divisions. Hexahedron elements [16] are employed, and numbers of the elements and the nodes employed are 2012 and 3235, respectively. The adhesive layer was divided into two meshes of 0.1 mm thickness in the x (thickness) direction after the effect and accuracy of the mesh divisions on the stress wave propagations and stress distributions were examined, taking account of the computational time. The finite element method (code name is DYNA3D [17, 18]) employed is explicit. In DYNA3D [17, 18], an initial velocity is provided as the initial condition. Figure 3 shows a joint in the case where the web length $2l_2$ is equal to the flange length $2l_1$ ($l_2 = l_1$ in Figure 1). The computations were performed for the joint shown in Figure 3 in order to examine the effect of the web length ($2l_2$) on the interface stress distributions. Sato and Ikegami [15] described the dynamic behavior of an epoxy adhesive subjected to impact loads. It is found that an increase in Young's modulus of the epoxy adhesive is very small under impact loads. Therefore, the viscoelasticity of the adhesive is not taken into consideration in our calculations. In the previous study [16], the effects of the mesh sizes and element division on the stress propagation and the stress distribution of joints under impact loads were examined. The number of divisions in the thickness direction of the adhesive layer was changed from 2 to 4, and the calculated results were compared. When the minimum thickness of element was chosen as the cases of 0.025 mm

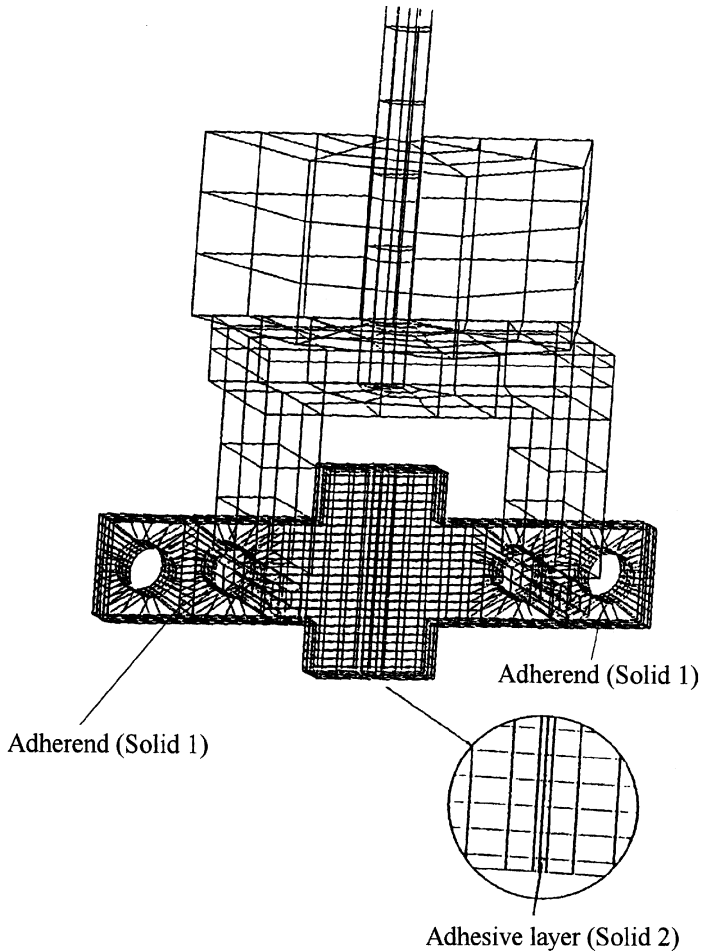


FIGURE 2 An example of mesh division in impact analysis for T-shaped butt adhesive joints.

(4 layers) and 0.05 mm (2 layers), it was confirmed that a difference in the calculated results of the interface stress distributions was very small. Thus, in this study, the minimum size of the elements is chosen as 0.05 mm in the FEM calculations.

EXPERIMENTAL METHOD

Figure 4 shows the dimensions of the specimen used in the strain response measurement. The specimens were made of aluminum, and

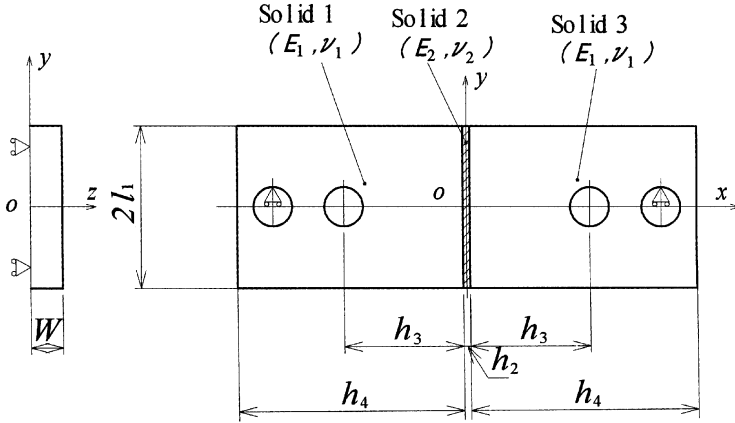


FIGURE 3 A model for FEM calculations in the case where web length $2l_2$ equals flange length $2l_1$.

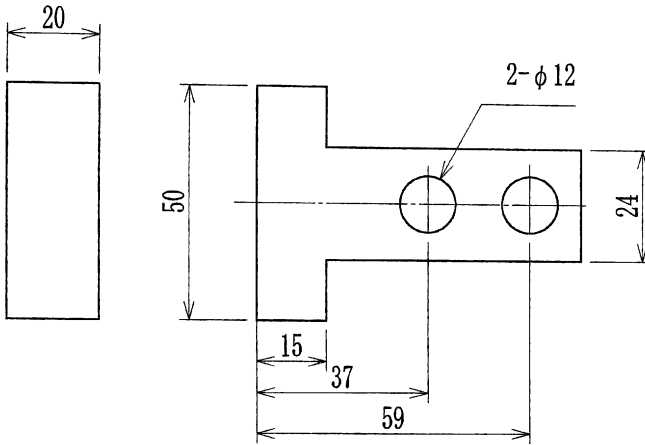


FIGURE 4 Dimension of T-shaped specimen used in the measurement.

they were joined by an epoxy adhesive of which Young's modulus was 3.63 GPa and Poisson's ratio was 0.38. The bonding process is as follows: (1) The surface impurities were removed using 2-butanone (methyl ethyl ketone, MEK), (2) the interfaces of the specimens were joined by the adhesive, and (3) the joint was cured at room temperature for 24 h.

Figure 5 shows a schematic of the experimental setup. The positions of the attached strain gauges are 2 mm from the interfaces and the

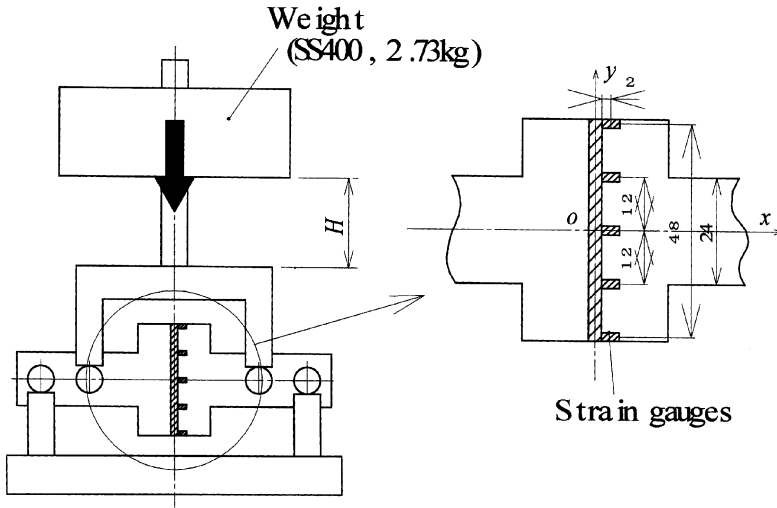


FIGURE 5 A schematic experimental setup for measuring strain response.

positions y are 24, 12, 0, -12 , and -24 mm from the center of the joint as shown in Figure 5. Strain gauges were attached in the x direction. A weight of 26.754 N (made of mild steel) was dropped from a height of $H = 200$ mm. The strain responses were recorded.

RESULTS OF FEM CALCULATIONS AND COMPARISONS BETWEEN CALCULATED AND MEASURED RESULTS

Results of FEM Calculations

In the FEM calculations, the dimensions and the material constants used are the same as those used in the strain response measurements (Figure 4). The initial velocity of the weight is chosen as $v = -1980$ mm/s (impact energy is 5.35 J) because the weight is assumed to drop from a height of $H = 200$ mm. When the stress propagation was examined in all the elements, it was found that the highest value of the maximum principal stress, σ_1 , occurred at the edge of $z = w$. Consequently, the stresses at $z = w$ is indicated hereinafter. The maximum principal stress, σ_1 , is described in this article because joint rupture is assumed to follow the maximum principal stress theory. The stress components are described in Figure 9 and 13.

Figures 6–9 show the results of FEM calculations for the T-shaped joint shown in Figure 4 ($l_1 = 25$ mm, $l_2 = 12$ mm). Figure 6 shows the maximum principal stress propagations at the positions $y = 25, -6,$

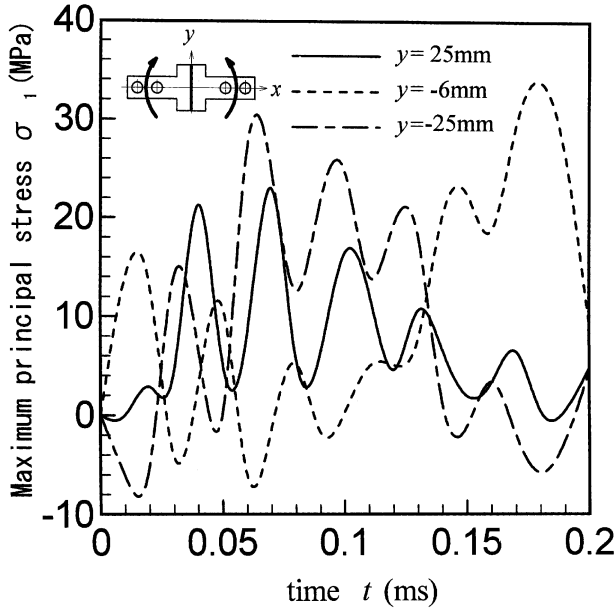


FIGURE 6 Maximum principal stress propagations at the interface ($x = h_2/2$, $z = w$) of T-shaped joints ($l_1 = 25$ mm, $l_2 = 12$ mm, $h_1 = 15$ mm, $h_2 = 0.1$ mm, $h_3 = 37$ mm, $E_1 = 69.6$ GPa, $E_2 = 3.6$ GPa, $\nu = -1980$ mm/s).

and -25 mm of the interfaces ($x = h_2/2$, $z = w$). The ordinate is the maximum principal stress, σ_1 , and the abscissa is the elapsed time, t . In this case, the stresses σ_1 were examined up to 0.6 ms of elapsed time, t ; however, the values of σ_1 decrease after 0.2 ms. Thus, the stresses are indicated up to 0.2 ms hereafter. It is observed that the maximum principal stress, σ_1 , becomes the highest value at the position $y = -6$ mm of the interface at the time of about 0.18 ms. Figure 7 shows the maximum principal stress, σ_1 , at the interfaces ($x = -h_2/2$, $z = w$) when the elapsed time t is 0.16 , 0.18 , and 0.19 ms. It is found that the maximum principal stress, σ_1 , is highest at $y = -6$ mm and the elapsed time $t = 0.18$ ms. In this study, a stress means the stress at the Gaussian point in an element. In addition, the interface stress shows at the Gaussian point of elements at the interface of the adhesive.

Figure 8 shows the maximum principal stress propagations at the interfaces ($x = \pm h_2/2$, $y = -6$ mm, $z = w$) and at the middle plane ($x = 0$, $y = -6$ mm, $z = w$) of the adhesive. It is observed that the maximum principal stress, σ_1 , becomes maximal at the interfaces. From the results, it can be concluded that the maximum principal

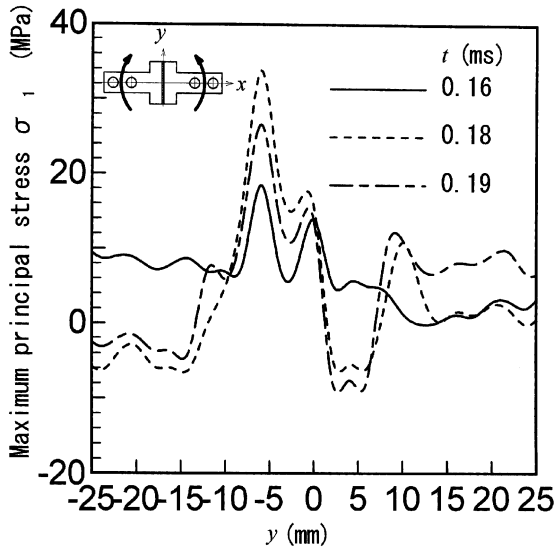


FIGURE 7 Maximum principal stress distributions at the interface ($x = h_2/2$, $z = w$) of T-shaped joints ($l_1 = 25$ mm, $l_2 = 12$ mm, $h_1 = 15$ mm, $h_2 = 0.1$ mm, $h_3 = 37$ mm, $E_1 = 69.6$ GPa, $E_2 = 3.6$ GPa, $\nu = -1980$ mm/s).

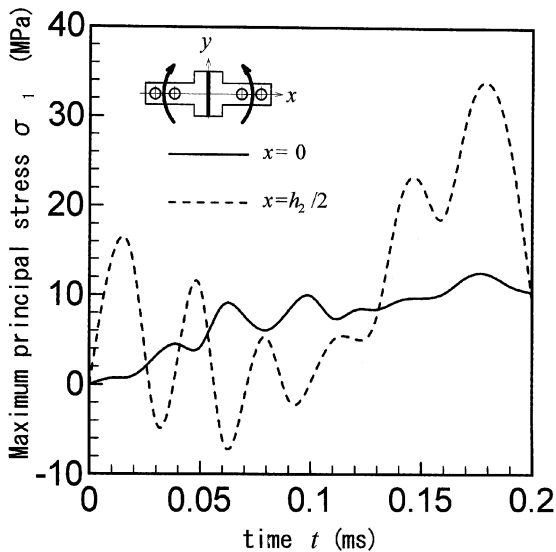


FIGURE 8 Maximum principal stress at the interface ($x = h_2/2$) and at the middle plane ($x = 0$) of adhesive ($l_1 = 25$ mm, $l_2 = 12$ mm, $h_1 = 15$ mm, $h_2 = 0.1$ mm, $h_3 = 37$ mm, $E_1 = 69.6$ GPa, $E_2 = 3.6$ GPa, $\nu = -1980$ mm/s).

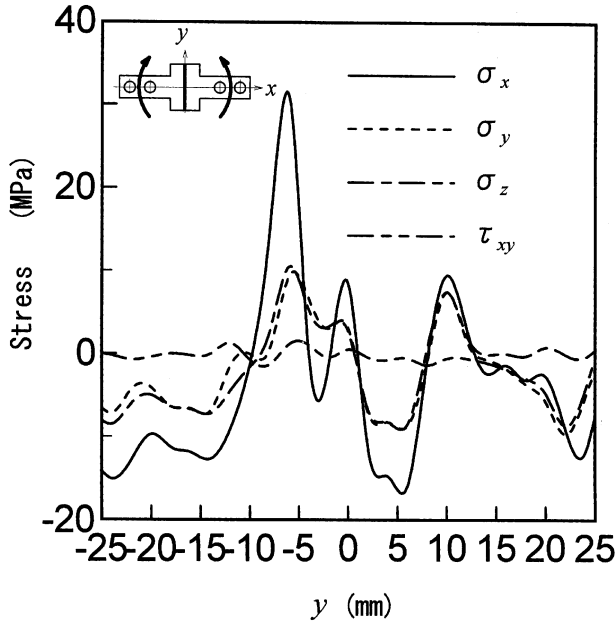


FIGURE 9 Distribution of each stress component at the interfaces and at elapsed time $t = 0.18$ ms ($x = \pm h_2/2$, $z = w$, $l_1 = 25$ mm, $l_2 = 12$ mm, $h_1 = 15$ mm, $h_2 = 0.1$ mm, $h_3 = 37$ mm, $E_1 = 69.6$ GPa, $E_2 = 3.6$ GPa, $v = -1980$ mm/s).

stress of T-shaped joints becomes maximal at the position $x = \pm h_2/2$ (interfaces), $y = -6$ mm, $z = w$. Figure 9 shows the distribution of stress components at the interfaces when the elapsed time is 0.18 ms. It is found that the stress component σ_x is the highest, while the normal stress component of which the direction is the same as the direction of impact loadings is substantial [14] when an impact tensile load is applied to the adhesive joints. Theoretically, the stress component σ_z must be zero at the boundary. However, as has been described before, the stress indicates at Gaussian point of elements along the edge of $z = w$. Thus, the stress component σ_z is not zero.

Figures 10–13 show the results of FEM calculations for the joint shown in Figure 3 when the web length, $2l_2$, is equal to the flange length, $2l_1$. Figure 10 shows the maximum principal stress, σ_1 , propagation at the positions $y = 25$, -6 and -25 mm of the interfaces ($\pm x = h_2/2$, $z = w$). It is found that the maximum principal stress σ_1 is highest at the edge ($y = -25$ mm) of the interfaces at the elapsed time of about $t = 0.11$ ms. In the previous paper [14], it was seen that the maximum principal stress σ_1 became maximal at the edge

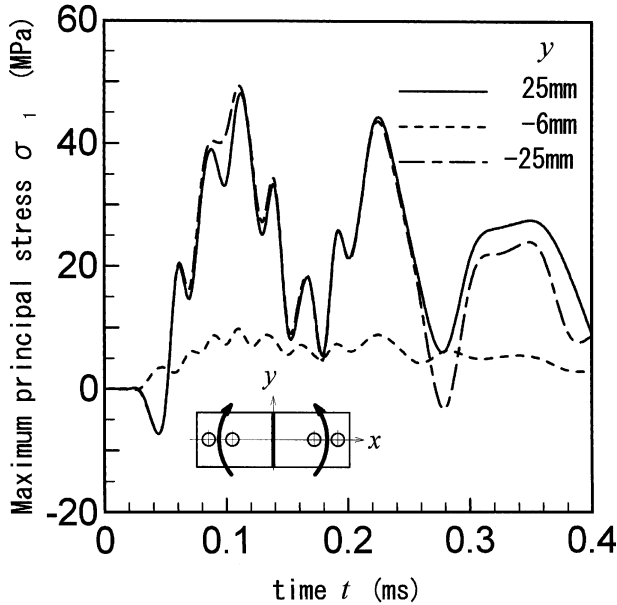


FIGURE 10 Maximum principal stress propagations at the interface ($\pm x = h_2/2$, $z = w$) in the special case where web length $2l_2$ equals to flange length $2l_1$ ($l_2 = l_1 = 25$ mm, $h_2 = 0.1$ mm, $h_3 = 37$ mm, $E_1 = 69.6$ GPa, $E_2 = 3.6$ GPa, $\nu = -1980$ mm/s).

($y = -25$ mm) of the interfaces when an impact tensile load was applied to the joint. Thus, it can be concluded that the effect of the web length ($2l_2$) on the interface stress distributions is substantial. In addition, from comparison with the results shown in Figures 7 and 8, it is found that the highest value of σ_1 is greater than that in Figures 7 and 8.

Figure 11 shows the maximum principal stress, σ_1 , at the interfaces ($\pm x = h_2/2$, $z = w$) when the elapsed time, t , is 0.10, 0.11, and 0.12 ms. When the elapsed time is 0.11 ms, the maximum principal stress is highest at the edge of the interfaces ($x = \pm h_2/2$, $y = -25$ mm, $z = w$). The tensile stress and compressive stress waves are different in phase. Thus, after superimposing each stress component at the tensile and the compressive sides, the maximum principal stress distributions are obtained as shown in Figure 11. In the special case where the web length equals the flange width, the stress wave propagation is different from that where the web length is not equal to the flange width (T-shaped adherends). Figure 12 shows the maximum principal stress propagation at the interfaces ($x = \pm h_2/2$, $y = -25$ mm, $z = w$) and at the

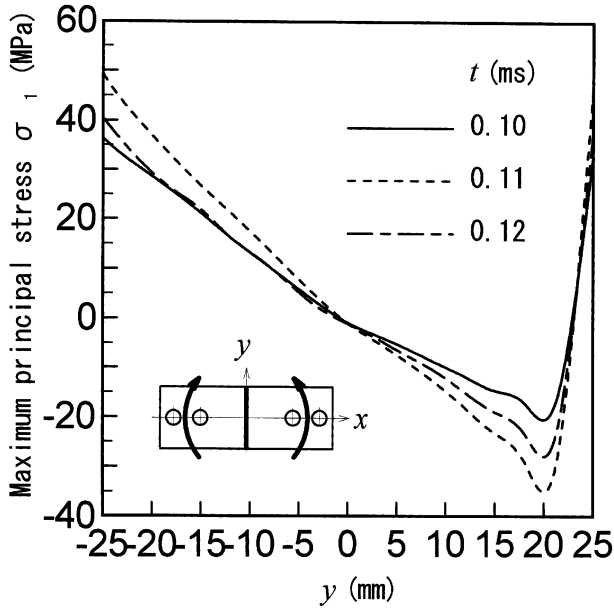


FIGURE 11 Maximum principal stress distributions at the interface ($x = h_2/2$, $z = w$) in the special case ($l_2 = l_1 = 25$ mm, $h_2 = 0.1$ mm, $h_3 = 37$ mm, $E_1 = 69.6$ GPa, $E_2 = 3.6$ GPa, $v = -1980$ mm/s).

middle plane ($x = 0$, $y = -25$ mm, $z = w$) of the adhesive. In this case, it is observed that the maximum principal stress also becomes maximal at the interfaces. From the results, the maximum principal stress in the special case shown in Figure 3 becomes highest at the edges of the interfaces, that is, $x = \pm h_2/2$, $y = -25$ mm, $z = w$. Figure 13 shows the distribution of stress components at the interfaces when the elapsed time is 0.11 ms. It is found that the stress component σ_x is substantial in this special case. Theoretically, the stress component σ_y must be zero at the boundary. However, as has been described before, the stress occurs at the Gaussian point of the elements along the edge of $y = \pm 25$ mm. Thus, the stress component σ_y is not zero at the free boundary. In addition, it is also emphasized that the stress distribution in this special case (Figure 13) is different from that shown in Figure 9 (T-shaped). The effect of the web length on the stress wave propagations and stress distribution at the interfaces is examined by FEM calculations. It was found that the position where the highest value of σ_1 occurred moved toward the edges of the interface ($x = \pm h_2/2$, $y = -25$ mm, $z = w$) under impact bending moments as the web length l_2 increased.

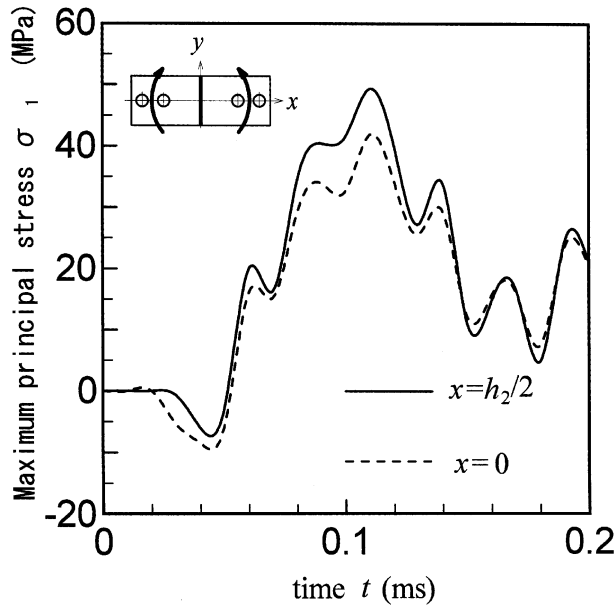


FIGURE 12 Maximum principal stress propagations at the interfaces ($x = \pm h_2/2$) and at the middle adhesion ($x = 0$) in the special case ($l_2 = l_1 = 25$ mm, $h_2 = 0.1$ mm, $h_3 = 37$ mm, $E_1 = 69.6$ GPa, $E_2 = 3.6$ GPa, $v = -1980$ mm/s).

This result is the same that as for the T-shaped adhesive butt joints under impact tensile loads [14]. In general, it is noticed that the stress waves propagate through the pins and they disperse at the flange end, and the reflections are repeated. Furthermore, the highest value of σ_1 increases as the web length l_2 increases under impact bending moments. This result is opposite to the result for the joints under impact tensile loads [14].

Figures 14 and 15 show the effect of Young's modulus, E_1 , of the adherends. The Young's modulus, E_2 , of the adhesive is held constant at $E_2 = 3.63$ GPa, and the value of E_1 is changed to 69.6, 137.2, and 205.8 GPa. Figure 14 shows the results in the case of T-shaped joints ($l_2 = 12$ mm). It is found that the highest value of the maximum principal stress, σ_1 , increases as the value of E_1 increases when Young's modulus E_2 of the adhesive is held constant. As Young's modulus of adherends, E_1 , decreases, the deformation in the web part of the adherends ($+h_2/2 + h_1 < x < h_3$, $-l_2 < y < +l_2$ and $-h_3 < x < -h_2/2 - h_1$, $-l_2 < y < +l_2$) increases, so the energy absorption capacity of the joints increases. Thus, when the same impact load is applied to the joints, as

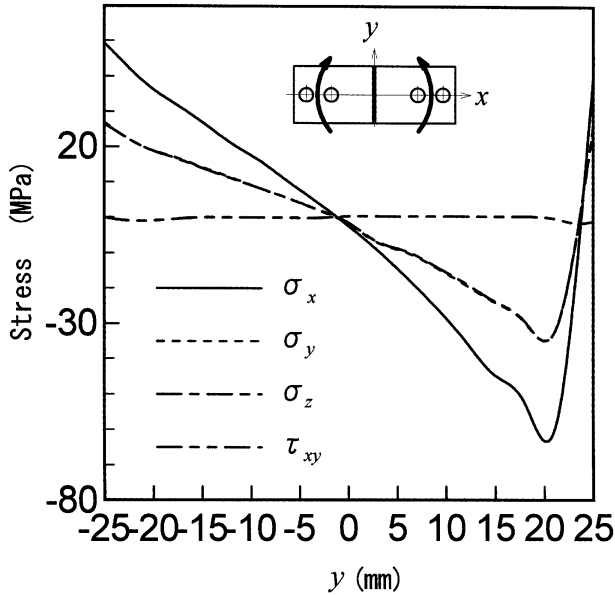


FIGURE 13 Each stress component at the interface ($\pm x = h_2/2, z = w$) and the elapsed time $t = 0.11$ ms in the special case ($l_2 = l_1 = 25$ mm, $h_2 = 0.1$ mm, $h_3 = 37$ mm, $E_1 = 69.6$ GPa, $E_2 = 3.6$ GPa, $v = -1980$ mm/s).

Young's modulus of adherends, E_1 , decreases, the highest value of the maximum principal stress, σ_1 , at the interfaces between the adherends and the adhesive layer decreases. In addition, it is assumed that the highest value of σ_1 increases as Young's modulus of the adhesive E_2 increases when Young's modulus E_1 of the adherend is held constant. Figure 15 shows the results for the special case ($l_1 = l_2$). It is assumed that as Young's modulus, E_1 , of adherends decreases, the deformation of the adherends increases where $+h_2/2 + h_1 < x < h_3, y = -l_1$ and $-h_3 < x < -h_2/2 - h_1, y = -l_1$. So, the singularity of stress at the edges of the interfaces ($x = +h_2/2, y = -l_1, z = w$ and $x = -h_2/2, y = -l_1, z = w$) between the adherends and the adhesive increases as the highest value of the maximum principal stress, σ_1 , increases. This result is the opposite of the result for Figure 14. It is assumed that as Young's modulus of adherends E_1 decreases, the deformation of the adherends where $+h_2/2 + h_1 < x < h_3, y = -l_1$ and $-h_3 < x < -h_2/2 - h_1, y = -l_1$ increases. So, the singularity of stress at the edges of the interfaces ($x = +h_2/2, y = -l_1, z = w$ and $x = -h_2/2, y = -l_1, z = w$) between the adherends and the adhesive increases as the highest value of the maximum principal stress increases.

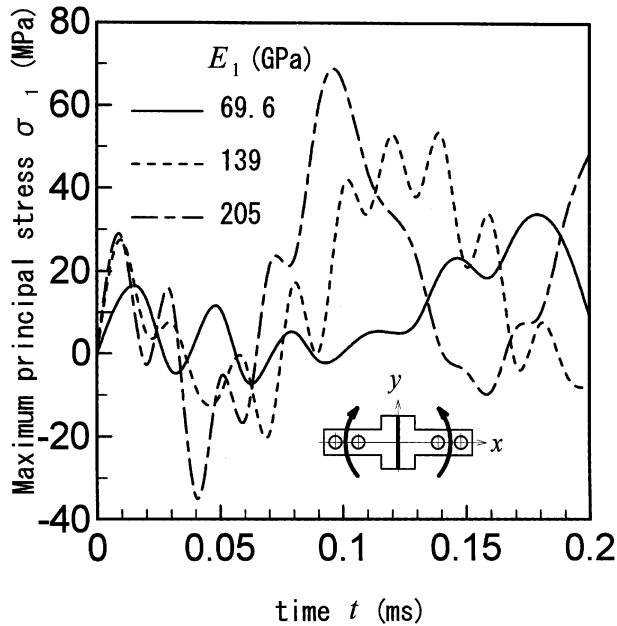


FIGURE 14 Effects of Young's modulus, E_1 , on the maximum principal stress at the interface ($x=h_2/2$, $y=6$ mm, $z=w$) in T-shaped joints ($l_1=25$ mm, $l_2=12$ mm, $h_1=15$ mm, $h_2=0.1$ mm, $h_3=37$ mm, $E_2=3.6$ GPa, $\nu=-1980$ mm/s).

Figures 16 and 17 show the effect of the adhesive thickness, h_2 , on the maximum principal stress, σ_1 . The adhesive thickness, h_2 , is changed to 0.1, 0.5, and 1.0 mm. It is observed that the value of σ_1 becomes maximal as the adhesive thickness decreases, both in the case of T-shaped (Figure 16) and in the special case (Figure 17). This is because the energy absorption performance increases as the adhesive thickness increases. In addition, this result is the same as for the joints under impact tensile loads [14]. In Figure 16, unstable behavior ($0 < t < 0.07$ ms) is found in the case of $h_2=0.1$ mm. This behavior is due to the side effect of flattening elements in DYNA3D.

Furthermore, the effect of joint dimensions on maximum principal stress propagation is examined by changing the joint proportion to 1.0 (basic model shown in Figure 4), 1.5 ($l_1=37.5$ mm, $l_2=18$ mm, $h_1=22.5$ mm, $h_2=0.15$ mm, $w=30$ mm) and 2.0 ($l_1=50$ mm, $l_2=24$ mm, $h_1=30$ mm, $h_2=0.2$ mm, $w=40$ mm). In the FEM calculations, the joint dimensions are changed and the calculations were done under the same conditions. In addition, it is also observed that

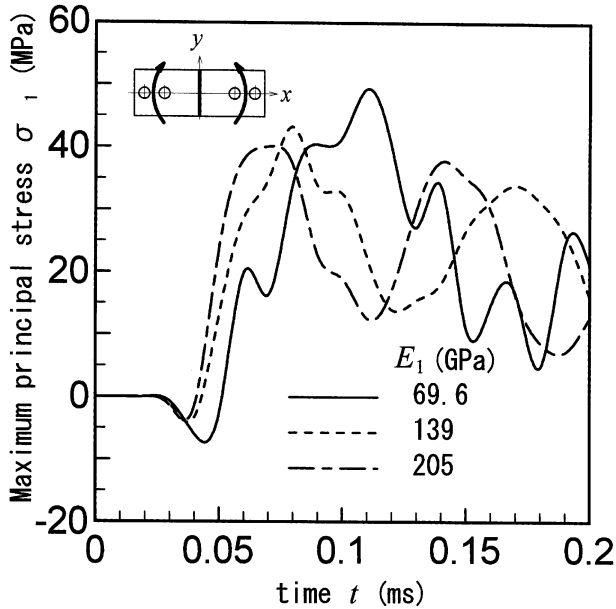


FIGURE 15 Effects of Young's modulus, E_1 , on the maximum principal stress at the interface ($x = h_2/2$, $y = -25$, $z = w$) in the special case ($l_2 = l_1 = 25$ mm, $h_2 = 0.1$ mm, $h_3 = 37$ mm, $E_2 = 3.6$ GPa, $v = -1980$ mm/s).

the position where the highest stress occurs moves from the center toward the edges of the interfaces as the dimensions of the T-shaped joint increases.

Comparisons of the Characteristics of the Joints Subjected to Impact and Static Bending Moments

The stress wave in the adhesive joint propagates under a quasistatic state. Stress wave reflection and interference are repeated, and the results on the obtained stresses are different from the stress state of joints subjected to static loadings. A T-shaped adhesive butt joint subjected to static bending moments was calculated by FEM. In the FEM calculations, the dimensions, the material constants, and the boundary conditions are the same as those used in the FEM calculations for the impact bending moments. However, in the model for FEM calculations, the static bending moment is applied to the ends of the T-shaped adherend as the linear static distributions. The code employed is MARC [20].

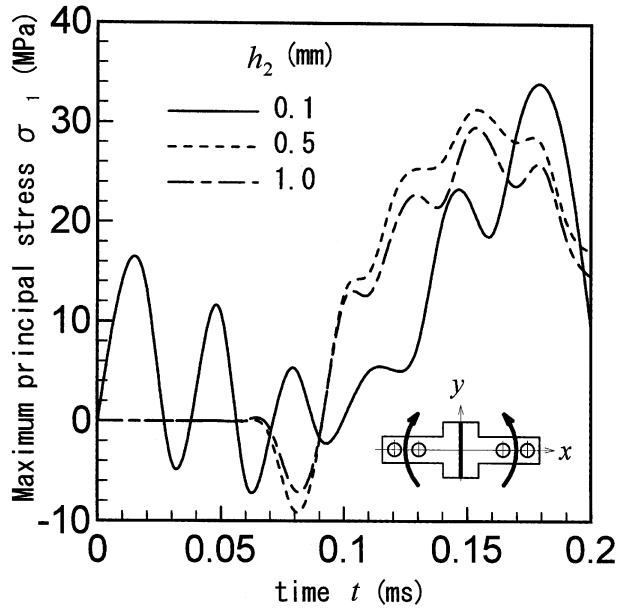


FIGURE 16 Effects of the adhesive thickness h_2 on the maximum principal stress at the interface ($x = h_2/2$, $y = 6$ mm, $z = w$) in the case of T-shaped joints ($l_1 = 25$ mm, $l_2 = 12$ mm, $h_1 = 15$ mm, $h_3 = 37$ mm, $E_1 = 69.6$ GPa, $E_2 = 3.6$ GPa, $v = -1980$ mm/s).

Figures 18 and 19 show the effect of Young's modulus, E_2 , of the adhesive. Young's modulus, E_1 , of the adherends is held constant at $E_1 = 69.6$ GPa, and the value of E_2 is changed to 3.6, 36, and 54 GPa. Figure 18 shows the results in the case of T-shaped joints ($l_2 = 12$ mm). It is found that the highest value of σ_1 occurs at the interfaces under the end of web ($y = 12$ mm, $z = 10$ mm), and it increases as Young's modulus, E_2 , of the adhesive increases. In addition, it is observed that the maximum principal stress, σ_1 , shows a tendency to become singular at the edges of the interfaces and it increases at the edge ($y = 25$ mm) as Young's modulus of the adhesive, E_2 , decreases. Figure 19 shows the results for the special case ($l_1 = l_2$). It is found that the highest value of the maximum principal stress, σ_1 , which occurs at the edges of the interfaces ($x = \pm 0.05$ mm, $y = 25$ mm, $z = 10$ mm) and shows singularity, becomes maximal as the value of E_2 decreases. The changes in the stress close to the singular point of $y = 25$ mm ($-23.5 < y < -25.0$ mm) are incorporated in Figure 19 (see inset) in order to enlarge the change in the singularity. This result is opposite

to the results for T-shaped adhesive joints subjected to impact bending moments.

Figures 20 and 21 show the effect of the adhesive thickness, h_2 . Figure 20 shows the results in the case of T-shaped joints ($l_2 = 12$ mm). The adhesive thickness h_2 is changed to 0.1, 0.5, and 1.0 mm. It is observed that the value of σ_1 becomes maximal at the interfaces ($x = \pm h_2/2$, $z = 10$ mm) under the end of the web ($l_2 = 2$ mm) as the adhesive thickness, h_2 , decreases, in the case of T-shaped joints (Figure 20). This result is same as the results for T-shaped adhesive joints subjected to impact bending moments. But in the special case ($l_2 = l_1$) (Figure 21), the value of σ_1 becomes maximal at the edge of the interfaces ($x = \pm h_2/2$, $y = 25$ mm, $z = 10$ mm) and it shows singularity. In addition, it is observed that the value of σ_1 increases as the adhesive thickness h_2 increases. This result is opposite to the results for the special case of T-shaped adhesive joints ($l_1 = l_2$) subjected to impact bending moments.

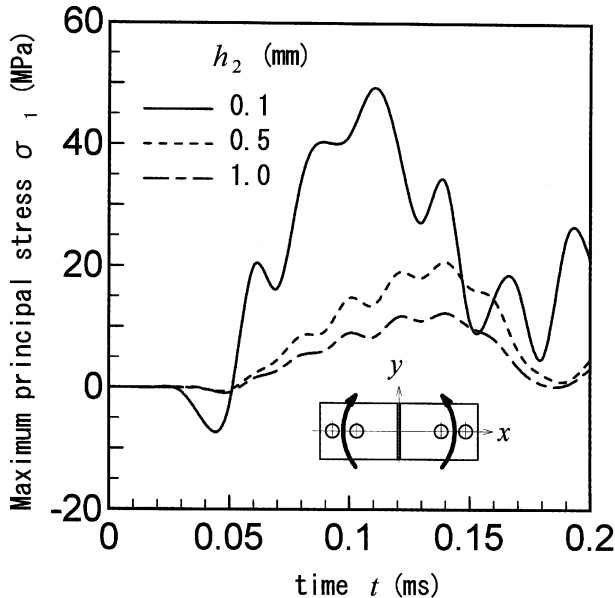


FIGURE 17 Effects of the adhesive thickness h_2 on the maximum principal stress at the interface ($x = h_2/2$, $y = -25$ mm, $z = w$) in the special case ($l_2 = l_1 = 25$ mm, $h_2 = 0.1$ mm, $h_3 = 37$ mm, $E_1 = 69.6$ GPa, $E_2 = 3.6$ GPa, $\nu = -1980$ mm/s).

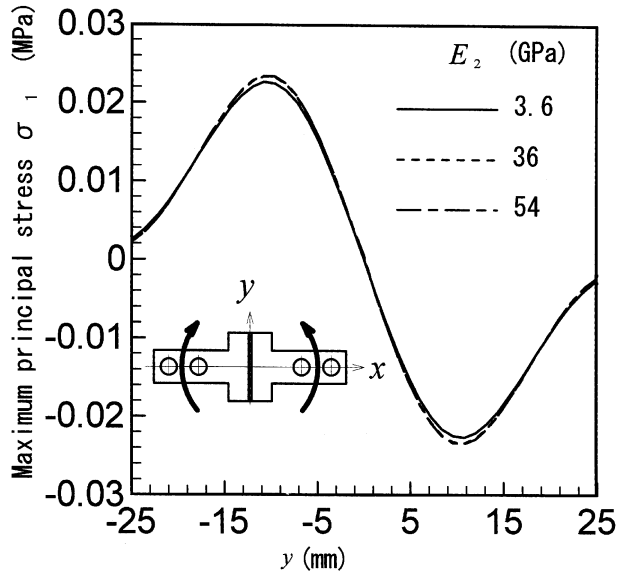


FIGURE 18 Effects of Young's modulus, E_2 , on the maximum principal stress distributions at the interfaces ($x = \pm h_2/2$, $z = w$) in T-shaped joints subjected to static bending moments ($l_1 = 25$ mm, $l_2 = 12$ mm, $h_1 = 15$ mm, $h_2 = 0.1$ mm, $h_3 = 37$ mm, $E_1 = 69.6$ GPa, $v = -1980$ mm/s).

Comparison Between the Numerical and the Measured Results on the Strain Response

Figure 22 shows the comparison of the strain response. The strain responses were measured at the positions of $y = 24$, 12 , 0 , -12 , and -24 mm shown in Figure 5. In Figure 22, the strain response at the positions of $y = 12$ mm is indicated. The ordinate is the strain, ϵ_x , in the x direction and the abscissa is the elapsed time, t . A fairly good agreement is observed between the numerical and the measured results.

CONCLUSIONS

In this article stress propagation and stress distribution were calculated by FEM (code name is DYNA3D) for T-shaped adhesive butt joints subjected to impact four-point bending moment of which the strain rate was small. The results obtained are as follows.

1. It is found that the highest value of the maximum principal stress, σ_1 , in T-shaped adhesive butt joints occurs at the interfaces, and it

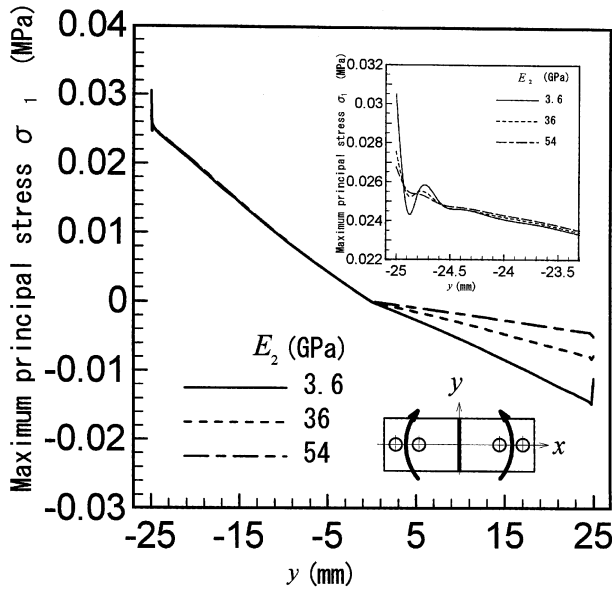


FIGURE 19 Effects of Young's modulus, E_2 , on the maximum principal stress distributions at the interface ($x = \pm h_2/2, z = w$) in the special case subjected to static bending moments ($l_2 = l_1 = 25$ mm, $h_2 = 0.1$ mm, $h_3 = 37$ mm, $E_1 = 69.6$ GPa, $\nu = -1980$ mm/s).

moves from the center toward the edge of the interfaces as the web length, $2l_2$, increases.

2. It is observed that the highest value of the maximum principal stress, σ_1 , increases as the value of E_1 (Young's modulus of adherends) increases in the case of T-shaped joints. In the case where the web length is equal to the flange length ($l_2 = l_1$), the highest value of σ_1 increases as the values of E_1 decreases.
3. It is observed that the highest value of σ_1 increases as the adhesive thickness, h_2 , decreases in the case of T-shaped joints. In the case where the web length is equal to the flange length ($l_2 = l_1$), the highest value of σ_1 increases as the value of h_2 decreases.
4. The effect of the joint dimensions on the maximum principal stress was examined. The maximum principal stress increases as the joint dimensions decrease. In addition, it is found that the position where the highest stress occurs moves from the center toward the edge of the interfaces as the dimensions of T-shaped joint increases.

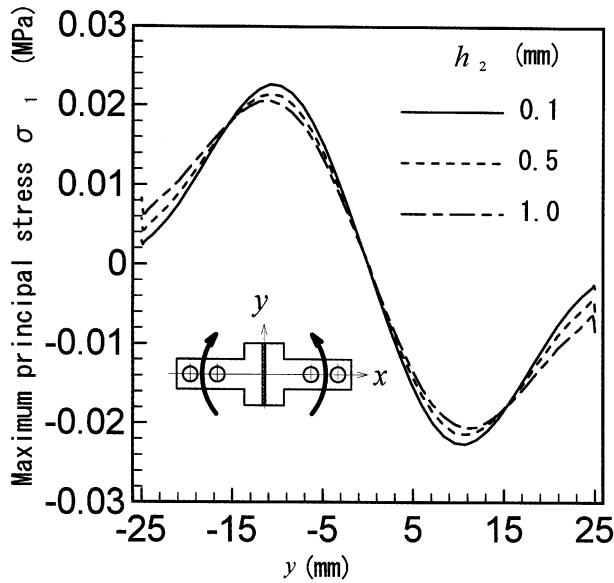


FIGURE 20 Effects of the adhesive thickness h_2 on the maximum principal stress distributions at the interfaces ($\pm x = h_2/2$, $z = w$) in the case of T-shaped joints subjected to static bending moments ($l_1 = 25$ mm, $l_2 = 12$ mm, $h_1 = 15$ mm, $h_3 = 37$ mm, $E_1 = 69.6$ GPa, $E_2 = 3.6$ GPa, $v = -1980$ mm/s).

5. The characteristics of the T-shaped joints under static bending moments were examined by FEM. The highest value of the maximum principal stress, σ_1 , increases as the value of Young's modulus E_2 (Young's modulus of adhesive) increases. In the special case ($l_1 = l_2$), the highest value of the maximum principal stress becomes maximal as the value of E_2 decreases. These results are opposite to the results for joints under impact bending moments.
6. The highest value of σ_1 becomes maximal as the adhesive thickness, h_2 , decreases in the case of T-shaped joints under static bending moments. This result is the same as the result for joints under impact bending moments. However, in the special case ($l_1 = l_2$) the highest value of σ_1 increases as the adhesive thickness increases. This result is opposite to the result for joints under impact bending moments.
7. Strain measurement on adherends was carried out. A fairly good agreement is observed between the measured and the numerical results.

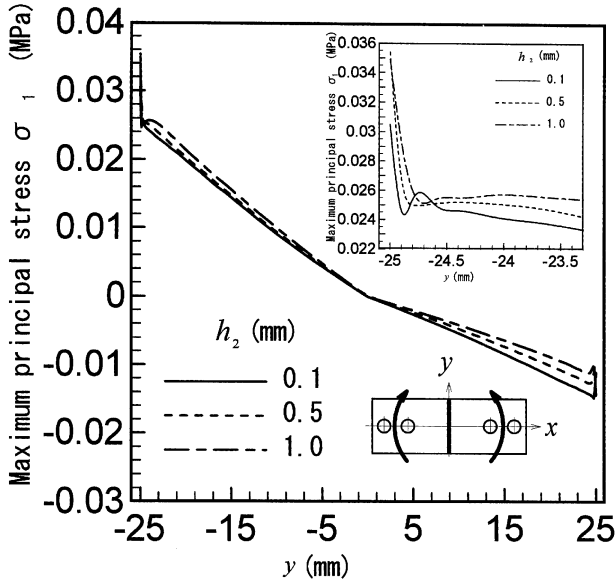


FIGURE 21 Effects of the adhesive thickness h_2 on the maximum principal stress distributions at the interfaces ($x = \pm h_2/2, z = w$) in the case subjected to static bending moments ($l_2 = l_1 = 25$ mm, $h_3 = 37$ mm, $E_1 = 69.6$ GPa, $E_2 = 3.6$ GPa, $v = -1980$ mm/s).

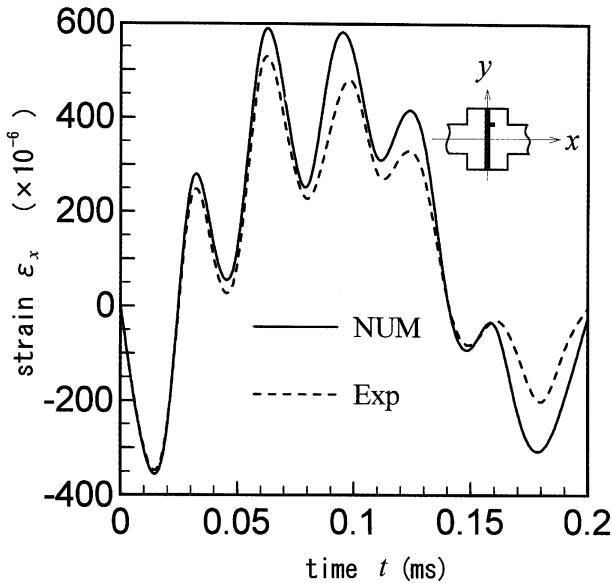


FIGURE 22 Comparisons between the numerical and the experimental results concerning strain response.

REFERENCES

- [1] Chen, D., *J. Applied Mechanics* **57**, 78–83 (1990).
- [2] Adams, R. D., *J. Adhesion* **30**, 219–242 (1989).
- [3] Tsai, M.-Y., and Morton, J., *J. Applied Mechanics* **61**, 712–715 (1994).
- [4] Sawa, T., Nakano, Y., and Temma, K., *J. Adhesion* **24**(1), 1–15 (1987).
- [5] Shi, Y. P., and Cheng, S., *J. Engineering Mechanics* **119**(3), 584–592 (1993).
- [6] Chen, D., and Cheng S., *J. Appl. Mech.* **50**, 109–115 (1983).
- [7] Brewis, D. M., *Materials Sci. Techno.* **2**, 761–773 (1986).
- [8] Sancaktar, E., Wei, Y., and Gaynes, M. A., *J. Adhesion* **56**, 229–246 (1996).
- [9] Yamada, S. E., *Eng. Fracture Mech.* **27**(3), 315–328 (1987).
- [10] Sawa, T., Temma, K., Nishigaya, T., and Ishikawa, H., *J. Adh. Sci. Technol.* **9**(2), 215–236 (1995).
- [11] Kinloch, A. J., and Kodokian, G. A., *J. Adhesion* **24**, 109–126 (1987).
- [12] Sawa, T., Seno, Y., Okuno, H., and Hagiwara, T., *J. Adhesion* **59**, 1–16 (1996).
- [13] Zachary L. W., and Burger, C. P., *Experimental Mechanics* **20**, 162–166 (1980).
- [14] Higuchi, I., Sawa, T., and Okuno, H., *J. Adhesion* **69**, 59–82 (1999).
- [15] Sato, C., and Ikegami, K., *Int. J. Adhesion Adhesive* **20**, 17–25 (2000).
- [16] Higuchi, I., Sawa, T., and Suga, H., *J. Adh. Sci. Technol.* **16**(12), 1585–1601 (2002).
- [17] Zhong, Z.-H., *Finite Element Procedures for Contact-Impact Problems* (Oxford Science Publications, 1993).
- [18] Hiroshima, T., and Sawa, T., *IMEchE, J. Strain Analysis* **31**(1), 43–58 (1996).
- [19] Hallquist, J. O., *User's Manuals for DYNA3D and DYNAP (Nonlinear Dynamic Analysis of Solids in Three Dimensions)* (University of California, Lawrence Livermore National Laboratory, Livermore, CA, Reprint UCID-19156, 1981).
- [20] *MARC User Manual*, Volume E, Part I, Version K7 (MARC Analysis Research Corporation, Palo Alto, CA, USA, 1997).